Improvement of Joint Strength of TC4/AZ91D Bimetal in Solid-liquid Compound Casting Process Using Cu-Ni Composite Interlayer

Fulin Wen[1] · Dengzhi Zheng[1] · Jianhui Liu[1]

Abstract

In the present study, the liquid-solid compound casting process has been developed for fabricating AZ91D/TC4 bimetal by adapting a Ni/Cu or Cu/Ni composite intermediate. The effects of interlayer sequence (Ni/Cu and Cu/Ni) on interface microstructure evolution and mechanical properties were investigated in detail. In particular, in order to promote interdiffusion of Cu and Ti elements at the Cu/Ti interface or Ni and Ti elements at the Ni/Ti interface, the vacuum heat-treat method was adapted before the liquid-solid compound casting process. The results showed that both the Ni/Cu and Cu/Ni composite interlayer realized metallurgical bonding between TC4 and AZ91D. The interface reaction layers of the TC4/AZ91D bimetal using Cu/Ni composite interlayer were composed of $Mg_2(Ni, Cu)$, Ni_2Mg_3Al, $Cu(Ni)$ solid solution and Mg-Ni eutectic structure. However, the interface reaction layers of TC4/AZ91D bimetal using the Ni/Cu composite interlayer were mainly composed of $Mg_2(Ni, Cu)$, $(Al_3Ni + Ni_2Mg_3Al)$ and Ni-Ti phases. Nano-indentation tests show that Ni-Ti intermetallic compounds has the highest nano-hardness at interface region, which leading to a poor shear strength at interface. When using Cu/Ni composite interlayer, the TC4/AZ91D bimetal had the highest shear strength of 97 MPa.

Keywords Bimetallic material · Liquid-solid compound casting · Interface intermetallic compound · Interface

1 Introduction

Magnesium alloys and titanium alloys have drawn the attention of aerospace, automotive, communication and energy fields as the perfect light materials for engineering application. The outstanding performance of Mg and its alloys, such as low specific density, high specific strength, good electromagnetic shielding effect, excellent damping performance and good recoverability were reported [1–3]. And, the Ti and its alloys also have some merits including higher specific strength than Mg alloy, good corrosion resistance, good fracture toughness and excellent high temperature performance [4, 5]. However, not only the application field of Mg and its alloys is limited due to its poor corrosion resistance and low high temperature strength but also the application field of Ti and its alloy is restricted because of high cost of manufacture of Ti alloys. Therefore, combing the performance features of Mg and Ti alloys to fabricate the Mg/Ti bimetals could meet the economic and performance requirements.

Many preparation methods have been performed on fabrication of Mg/Ti bimetals including friction stir welding, laser welding, spot welding, transient liquid phase (TLP) bonding process and liquid-solid compound casting process. Zhang et al. [6] fabricated Mg/Ti bimetals by laser welding brazing (LWB) method . Aonuma et al. [7] manufactured Ti (TA2) and Mg-Al-Zn composite using friction stir welding method. Gao et al. performed laser welded process to obtain AZ31B/TC4 butt joints [8]. Cao used cold metal transition welding technology method to bond the AZ31B and TA2 [9]. Differ from these methods mentioned above, Mg/Ti bimetals manufactured by liquid-solid compound casting process also shows many advantages. Firstly, the process procedure is sample and the energy input is low during the compound casting process. Secondly, casts could be fabricated with complex shape and large size. Additionally, external environment field such as vacuum, pressure and electromagnetism can be added during the casting process to adjust solidification structure [10–12]. Therefore, it

---

✉ Fulin Wen
  wfl_cqu@163.com

1   Institute of Machinery Manufacturing Technology China
    Academy of Engineering Physics, Mianyang,
    Sichuan 621900, PR China

is of great significance to explore then fabrication of Mg/Ti bimetals by solid-liquid compound casting process.

The most challenging thing is that there is no intermetallic compound (IMC) or solid solution formed between the interface of Ti and Mg based on the Mg-Ti binary phase diagram [8]. Generally, adapting an intermediate metal interlayer between Mg and Ti is an effective method to realize metallurgical bonding during the fabrication process of Mg/Ti bimetal. These intermediate metal interlayers including Zn, Al, Ni and Cu were often be selected and proved to be useful during the bonding process of Mg and Ti. Kaiping Zhang et al. [13] prepared immiscible and nonreactive Mg/Ti joints by laser heat-conduction welding process using Ni electro-coating as the intermediate metal interlayer and the reliable joint with metallurgical bonding between Mg/Ti was obtained. Atieh et al. [14] adapted Ni foil as the intermediate interlayer during the diffusion bonding of Mg to Ti alloy. The Mg-Ni eutectic products and Ni-Ti intermetallic compounds (IMCs) were observed at the interface region. After that, the Ni foil was replaced by Ni coating in a follow-up to their studies, and higher shear strength was obtained. Zang C et al. [15]. reported the immiscible Mg/Ti bonding by laser heat conduction technique using Al intermetallic interlayer and the $TiAl_3$ phase was observed at the interface region. Liu et al. [16] performed butt laser welding-brazing of Mg to Ti adapting Cu intermediate metal interlayer. With the increase of Cu coating thickness, metallurgical bonding was obtained between Mg/Ti due to the generation of $(Ti_3Al + Ti_2Cu + AlCu_2Ti)$ mixed tissue at the interface region. S.T. Auwal et al. [17] developed a fiber laser welding-brazing procedure to join the AZ31B/TC4 using a Cu-Ni intermediate metal interlayer. The results show that the Cu-Ni intermediate metal interlayer promotes wetting of the AZ92 filler on TC4 surface and the generation of reactions layers at the interface region are closely related to the interlayer arrangements. However, few researches have reported for the adaption of intermediate metal interlayer in the solid-liquid compound casting process of Mg/Ti bimetal. Cu and Ni are regard as the most widely used metal have many excellent properties such as thermal conductivity, toughness and ductility [18]. Meanwhile, these two metals can not only react with Ti and Mg to realize metallurgical connection but also can form an infinite solid solution according to the binary Cu-Ni phase diagram. However, the effects mechanism of Cu-Ni intermediate metal interlayer on the evolution of interface microstructure and mechanical properties of Mg/Ti bimetal are still indistinct. Further investigations of a new Cu-Ni composite interlayer is a promising attempt to improve the performances of the Mg/Ti bimetals.

In this study, a composite Cu/Ni or Ni/Cu metal interlayer were coated on the TC4 rod to fabricate the Mg/Ti bimetals. Vacuum heat treatment was performed on the Ni/Cu or Cu/Ni coated TC4 rods. After that, liquid-solid compound casting process was conducted and the effects of composite Ni/Cu or Cu/Ni metal interlayer on the evolution of interface microstructure and mechanical properties of Mg/Ti bimetal were investigated. Meanwhile, the reaction layers generation sequence and interface failure procedure was analyzed.

2 Experimental

2.1 Materials

TC4 titanium alloy rod with a chemical composition of Ti-5.82Al-4.81 V (wt%) was chosen as the solid insert. AZ91D magnesium alloy with a chemical position of Mg-9.58Al-0.75Zn (wt%) was melted as the liquid material.

2.2 Electroplating Process of Cu/Ni or Ni/Cu Interlayer

The Cu/Ni or Ni/Cu composite interlayer was prepared on the surface of TC4 rod by electroplating. Prior to electroplate, the surface of TC4 rod with a diameter of 5 mm was polished to 800 mesh using SiC sandpaper. After that, the electroplating Ni and Cu processes were performed. The electroplating process and chemical solution used in this job were described in our previous studies in detail [19, 20]. For electroplating process of Cu and Ni, all the electroplating time was set as 40 min. The schematic illustration and the structure of coatings are shown in Fig. 1. In order to strengthen the metallurgical bonding between TC4 substrate and (Cu, Ni) composite interlayer, the pre-vacuum heat treatment was adapted in this study under a vacuum degree of $3.0*10^{-3}$ Pa to avoid oxidization, and the vacuum heat treatment process parameter was set as 700 °C for 3 h.
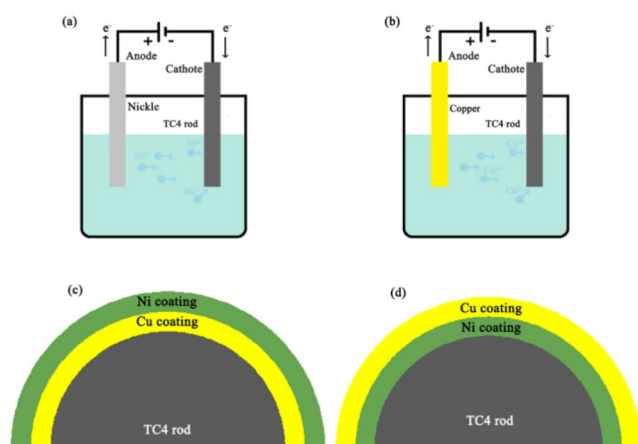

Fig. 1 The schematic illustration and the structure of coatings on TC4 rod

2.3 Liquid-solid Compound Casting Process

Figure 2 shows schematic of the liquid-solid compound casting process of TC4/AZ91D bimetal. In this work, AZ91D ingots were melted in the resistance furnace and covered by the RJ-2 flux to avoid oxidation during the melting process. The Ni/Cu or Cu/Ni covered TC4 rods were inserted in the metal mould and both of them were placed in the box-type furnace to preheat to 250 °C for 2 h. Then, the AZ91D melt was poured into the mould from the alumina crucible when its temperature come to 720 ± 5 °C. The TC4/AZ91D bimetal could be obtained after AZ91D melt solidified totally.

2.4 Microstructure and Mechanical Properties Testing

The metallographic samples were prepared based on standard metallographic preparation procedures. The interface microstructure of TC4/AZ91D bimetal was observed by a scanning electron microscope (SEM, TESCAN VEGAN-3 LMH) conducted with energy dispersive spectrometer (EDS). The shear strength of TC4/AZ91D bimetals were measured by CMT6305-300 KN universal tensile testing machine with a loading rate of 0.5 mm/min and the schematic sketch of the shear tester was shown in Fig. 3. At least 3 tensile shear testing samples were used to evaluate the shear strength of TC4/AZ91D bimetals. A nano indenter 6200 indentation tester was also used to measure nano hardness and elasticity modulus of the matrix and interface of TC4/AZ91D bimetals.

3 Results and Discussion

3.1 Microstructure and Compositions of Cu/Ni or Ni/Cu Composite Interlayer

The composite interlayer with different sequence strategies of Cu and Ni were prepared for liquid-solid compound casting of TC4/AZ91D bimetal. Figure 4 shows the cross section morphology and EDS results of the Ni/Cu or Cu/
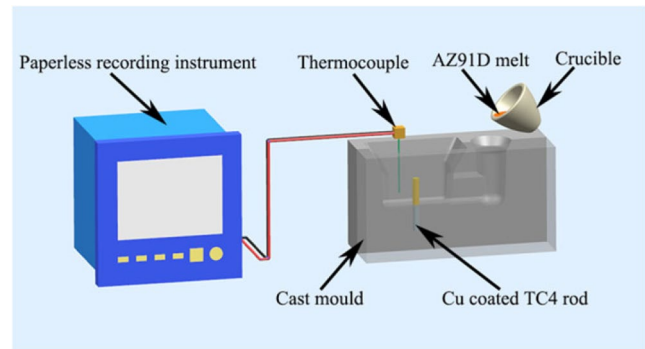

Fig. 2 Schematic illustration of the compound casting process

Ni coated TC4 rods. As can been seen, the dense composite interlayer of about 29.2 μm and 17.2 μm in total width are observed on the surface of TC4 rod. For the Cu/Ni composite interlayer, it consists of a Cu interlayer of about 24 μm on the surface of TC4 rod but a Ni interlayer of about 5.2 μm on the outside as shown in Fig. 4a, b. For the Ni/Cu composite interlayer, it consists of a Ni interlayer of about 8 μm on the surface of TC4 rod but a Cu interlayer of about 9.2 μm on the outside as shown in Fig. 4c, d. Although the electroplating time of Cu and Ni layer are both set as 40 min, the difference in thickness of Cu and Ni interlayer may be ascribed to the efficiency of electroplating for Cu and Ni at different substrate conditions.

3.2 Interface Microstructure of TC4/AZ91D Bimetal Coated with Cu/Ni or Ni/Cu Composite Interlayer

Before solid-liquid compound casting, the vacuum heat treatment of composite interlayer coated TC4 rods were performed to promote the inter-diffusion between composite interlayer and TC4 substrate. Figure 5 exhibits the cross section morphology and EDS results of composite Cu/Ni and Ni/Cu coated TC4 rods which are treated at 700 °C for 3 h. In Fig .5a, several Cu-Ti diffusion reaction layers generated at the interface of TC4/(Cu/Ni) interlayer substrate. In addition, Cu element was observed in this region to diffuse through the Ni interlayer and to gather at the surface of TC4 rod which leading to the generation of Ni (Cu) solid solution. EDS spot analysis result of P1 shows that Ni (Cu)

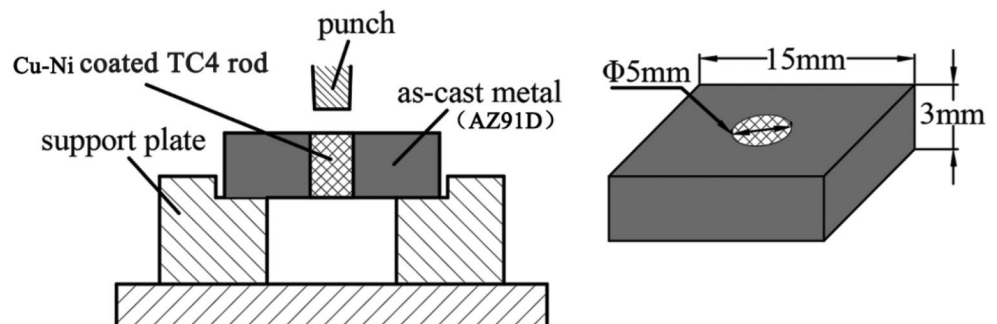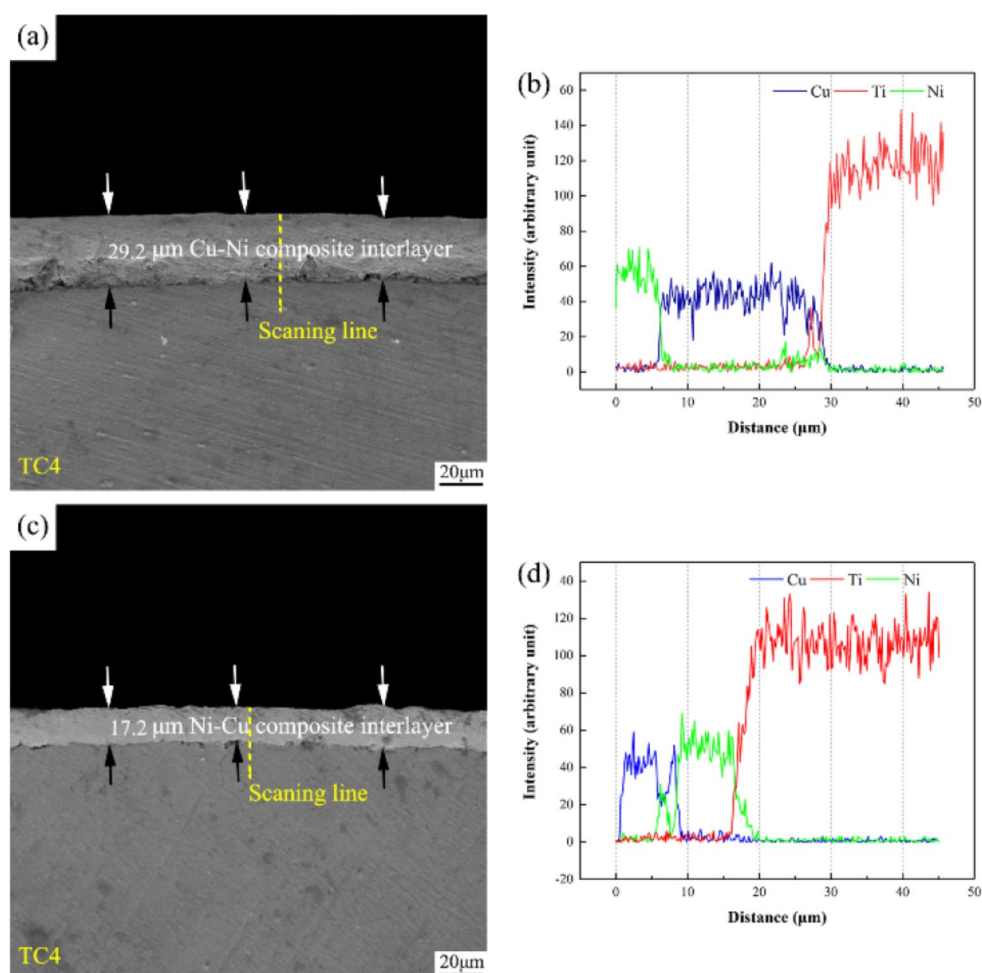**Fig. 3** Schematic of shear tester and the dimension of the shear test sample

Fig. 4 The cross section morphology and EDS results of Cu-Ni composite interlayer coated on TC4 rods: (**a**) TC4/(Cu/Ni), (**b**) EDS line scan results in a, (**c**) TC4/(Ni/Cu), (**d**) EDS line scan results in c

solid solution has an atomic composition of 61.51 at% Ni and 38.49 at% Cu. However, between the diffusion reaction layer of Cu-Ti system and the reaction layer of Ni (Cu) solid solution, there are still residual Cu layers which did not fully involve in the interfacial reaction.

Figure 5c shows the cross section morphology and EDS results of composite Ni/Cu coated TC4 rods. As shown, various reaction layers generated at Ni-Ti interface which can be confirmed as Ti_2Ni and Ni_3Ti phases based on the EDS line scan and point scan results as shown in Fig. 5b; Table 1. Differ from Fig. 5a, there are no Cu-Ti phases generate at the interface of TC4/(Ni/Cu) composite interlayer. In contrast, obvious inter-diffusion is observed between Ni and Cu interlayer at the surface of TC4 rod, resulting the generation of Cu (Ni) solid solution which has an atomic composition of 15.54 at% Ni and 84.46 at% Cu as shown in Table 1.

3.3 Constituent Phases at the Interfaces of TC4/AZ91D Bimetals

To determine the interface structure of TC4/AZ91D bimetals, the X-ray diffraction was used to analyze the constitutive

phases at interface zone and the results were illustrated in Fig. 6. As can be seen, the interfacial zone of the bimetallic materials fabricated using Cu/Ni or Ni/Cu composite interlayer were completely different. Cu-Ti IMCs, Mg-Al-Ni ternary phase and Mg-Ni phase were found fabricated by Cu/Ni composite interlayer, but Ni-Ti IMCs, Al-Ni and Mg-Al-Cu ternary compound were only found in the interface of TC4/AZ91D bimetallic castings manufactured using Ni/Cu composite interlayer.

3.4 Interface Microstructure of TC4/AZ91D Bimetals

The evolution of interface structure of TC4/AZ91D bimetals were investigated. Figure 7 displays the interface microstructure and EDS results of TC4/AZ91D bimetals fabricated using Cu/Ni composite interlayer. As shown, a width of 100 μm interface generated at the interface region. Except for the Cu-Ti reaction layers adjacent to TC4 matrix, a dense and uniform interface reaction layer is observed at the substrate of AZ91D alloy, indicating that metallurgical bonding is obtained between AZ91D/TC4 bimetal. Figure 7g and **h** illustrates the high magnification SEM images

Fig. 5 BSE micrographs of the Cu-Ni composite interlayer treated by 700 °C for 3 h: (**a**) TC4/(Cu/Ni), (**b**) high magnification SEM image of areas A in a, (**c**) EDS line scan results in a, (**d**) TC4/(Ni/Cu), (**e**) high magnification SEM image of areas B in d, (**f**) EDS line scan results in d
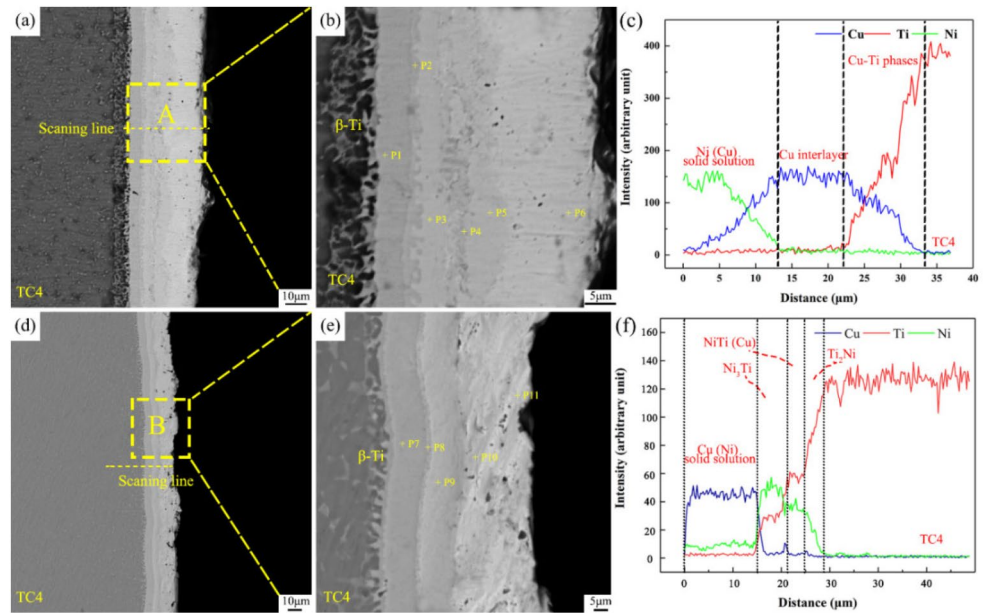

Table 1 EDS analysis results at different positions in Fig. 5

Point No.	Element compositions (at%)			Possible phases	Point No.	Element compositions (at%)			Possible phases
	Cu	Ni	Ti			Cu	Ni	Ti	
P1	35.24	--	64.76	CuTi$_2$	P7	--	35.11	64.89	NiTi$_2$
P2	48.52	--	51.48	CuTi	P8	8.54	41.36	50.1	NiTi (Cu)
P3	62.35	--	37.65	Cu$_4$Ti$_3$	P9	--	76.28	23.72	Ni$_3$Ti
P4	75.36	--	24.64	Cu$_4$Ti	P10	82.53	17.47	--	Cu (Ni)
P5	94.32	5.68	--	Cu	P11	80.46	19.54	--	Cu (Ni)
P6	80.52	19.48	--	Ni (Cu)					

Fig. 6 Constituent phases at the interfaces of TC4/AZ91D bimetals using (Cu-Ni) composite interlayer: (**a**) Cu/Ni, (**b**) Ni/Cu
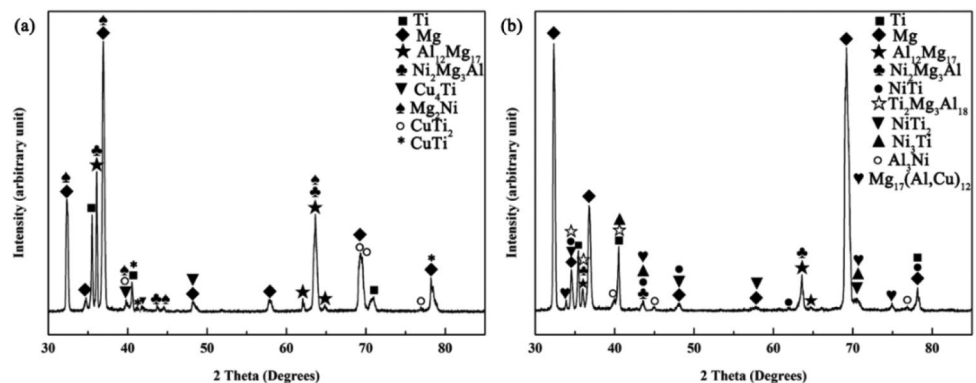
corresponding to region A and B in Fig. 7a, and the correlative EDS spot scan analysis results of **P1-P5** are listed in Table 2. As shown, **P1** on the gray reaction layer contains 12.84 at% Ni, 10.88 at% Cu and 76.28 at% Mg, indicating that this gray reaction layer is Mg$_2$(Ni, Cu) phase. The composition of **P2** is mainly 8.96 at% Ni, 6.99 at% Cu, and 84.05 at% Mg, which can be confirmed as the Mg-Ni eutectic structure phase.

Figure 7i show the EDS line scan results of the scanning line marked in Fig. 7g. As shown, Cu (Ni) solid solution was separated by Mg$_2$(Ni, Cu) phase from AZ91D matrix.

In other words, Mg$_2$(Ni, Cu) phase is the reaction product of Cu (Ni) solid solution and AZ91D melt. For Fig. 7h, it shows the high magnification SEM images of region B in Fig. 7a. The EDS compositional analysis revealed that **P3** is composed of 15.04 at% Al, 29.09 at% Ni, and 55.87 at% Mg, and **P4** is 14.03 at% Al, 19.36 at% Ni, 3.92 at% Cu and 62.69 at% Mg, which suggests that this reaction layer generates at the AZ91D matrix is the mixture of Mg-Al-Ni ternary phase and (Mg-Ni) eutectic structure. Between Cu-Ti IMCs and (Mg-Ni) eutectic structure, there are residual Cu(Ni) solid solution and Cu interlayer as shown for **P5 and P6**.

Fig. 7 SEM micrographs of the interface of TC4/(Cu/Ni)/AZ91D bimetals: (**a**) general view, (**b**)-(**f**) EDS mapping scan results in a, (**g** and **h**) areas A and B in (**a**), (**i**) EDS line scan results in (**g**)
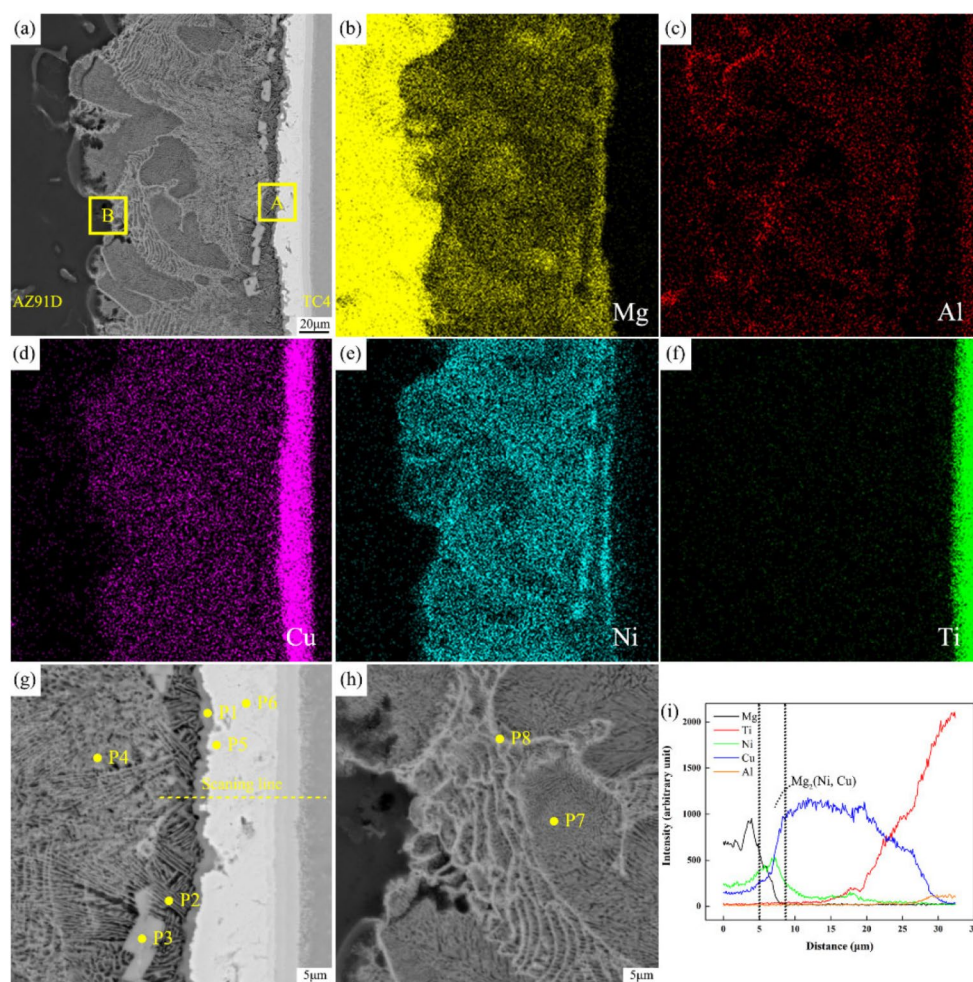

Table 2 EDS analysis results corresponding to points marked in Fig. 7

Point No.	Element compositions (at%)					Possible component
	Mg	Cu	Al	Ni	Ti	
P1	76.28	10.88	--	12.84	--	Mg$_2$(Ni, Cu)
P2	84.05	6.99	--	8.96	--	α-Mg + Mg2Ni
P3	55.87	--	15.04	29.09	--	Ni$_2$Mg$_3$Al
P4	62.69	3.92	14.03	19.36	--	Ni$_2$Mg$_3$Al
P5	5.06	59.04	--	35.90	--	Cu (Ni) solid solution
P6	4.48	96.52	--	--	--	Cu
P7	79.06	4.71	4.72	11.51	--	α-Mg + Mg$_2$Ni
P8	55.36	2.95	14.64	27.04	--	Ni$_2$Mg$_3$Al

These results were in accordance with XRD phase retrieve result. But the Mg-Ni eutectic structure phase and Ni$_2$Mg$_3$Al phase in this study was smaller and denser compared with our previous studies [21]. Based on the distribution of Cu element in the interface region, indicating that Cu atom can refine Mg-Ni eutectic structure effectively.

Figure 8 illustrates the interface microstructure of TC4/AZ91D bimetal manufactured using Ni/Cu composite interlayer. As shown, a width of 40 μm interface forms at the interface region. The reasons why the width of interface was different when using Cu/Ni and Ni/Cu composite mainly attributed to the thickness of Cu/Ni composite interlayer is thicker than that of Ni/Cu composite interlayer, thus offered more Cu and Ni atoms to participate interface reaction during solid-liquid compound casting of TC4/AZ91D. Meanwhile, a dense reaction layer which consists of granular phase can also be observed at AZ91D matrix besides Ni-Ti reaction layers. Figure 8c-g display the EDS map scanning results of Mg, Al, Cu, Ni and Ti elements at the same position of Fig. 8b. As shown, Al, Cu and Ni elements tend to

Fig. 8 SEM micrographs of the interface of TC4/(Ni/Cu)/AZ91D bimetals: (**a**) general view, (**b**) areas C in a, (**c**)-(**g**) EDS mapping scan results in (**b**), (**h**) area D in (**a**), (**i**) EDS line scan results in (**b**)
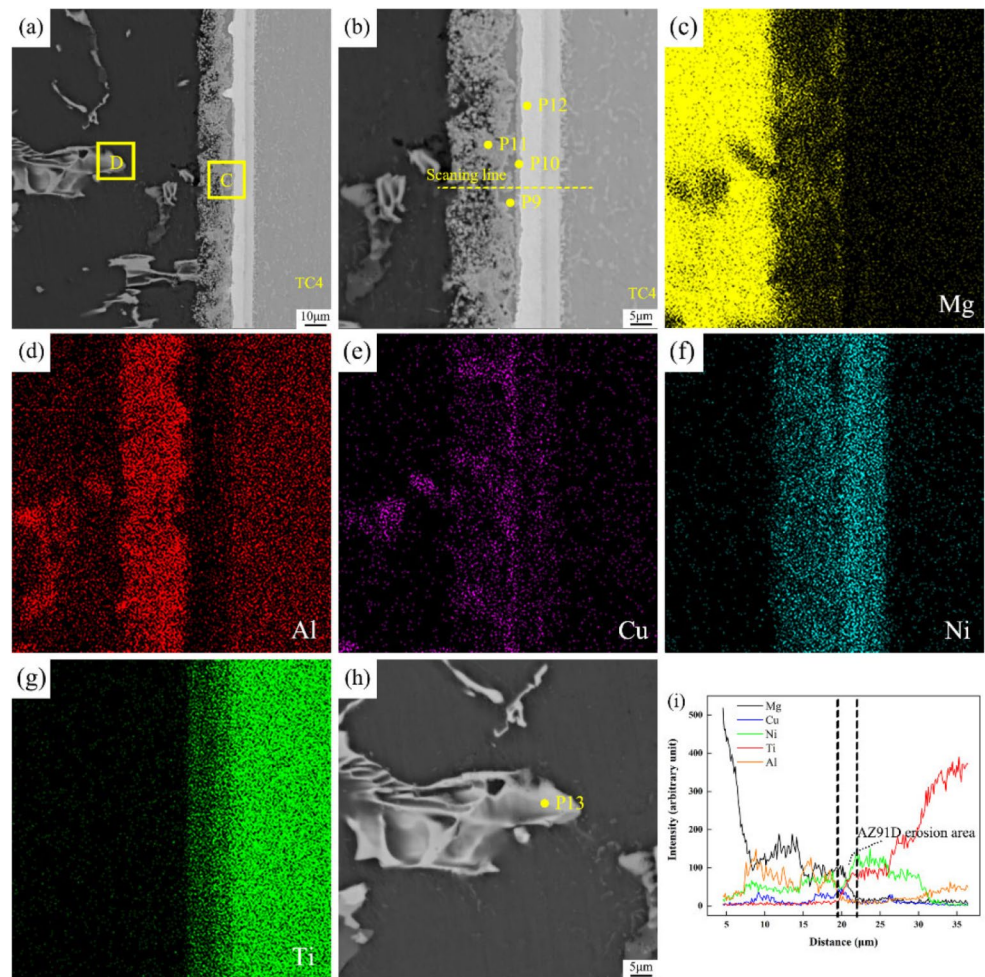

Table 3 EDS analysis results corresponding to points marked in Fig. 8

Point No.	Element compositions (at%)					Possible component
	Mg	Cu	Al	Ni	Ti	
P9	62.84	21.12	3.26	12.78	--	$Mg_2(Ni, Cu)$
P10	24.26	4.82	46.18	6.04	18.47	$Ti_2Mg_3Al_{18}$
P11	15.56	5.45	50.58	28.41	--	$Al_3Ni + Ni_2Mg_3Al$
P12	1.11	1.27	1.59	68.79	27.24	Ni_3Ti
P13	70.53	16.83	12.64	--	--	$Mg_{17}(Al, Cu)_{12}$

segreagate at the same position of AZ91D matrix, but Ti element appears gradient distribution at the interface region, illustrating that the metallurgical bonding forms at the interface of TC4/AZ91D bimetal. Figure 8h shows the high magnification SEM image of region C corresponding to Fig. 8a. The EDS spot scan analysis results of P9-P13 are listed in Table 3. It is found that **P9** is composed of 12.78 at% Ni, 21.12 at% Cu, 62.84 at% Mg and 3.26 at% Al, which may be $Mg_2(Ni, Cu)$ ternary phase. The chemical composition of **P10** on the gray reactive layer is 6.04 at% Ni, 4.82 at% Cu, 24.26 at% Mg, 46.18 at% Al and 18.47 at% Ti, which may be Ti-Mg-Al ternary phase, as indicated by Lv et al [21]. It can be found that **P11** (granular phase) contains

28.41 at% Ni, 5.45 at% Cu, 15.56 at% Mg and 50.58 at% Al, which suggests Mg-Al-Ni and Al-Ni mixed structure. For Ni-Ti reaction layers, they can be confirmed as Ti_2Ni and Ni_3Ti due to the chemacial composition of **P12** as listed in Table 3. Figure 8h shows the high magnification SEM image of region D corresponding to Fig. 8a. The chemical composition of **P13** is 16.83 at% Cu, 70.53 at% Mg and 12.64 at% Al, suggesting that this phase is Mg-Al-Cu ternary structure [22].

Fig. 9 The indentation morphology of the interface microstructure of TC4/(Cu/Ni)/AZ91D bimetals: (**a**) optical images, (**b**)-(**g**) laser confocal morphology
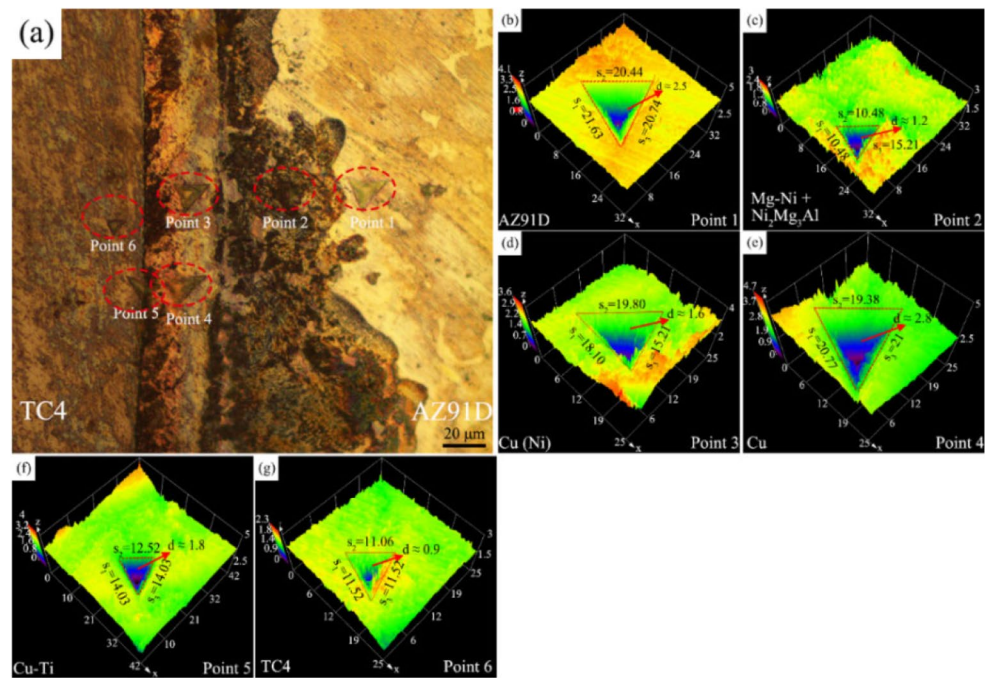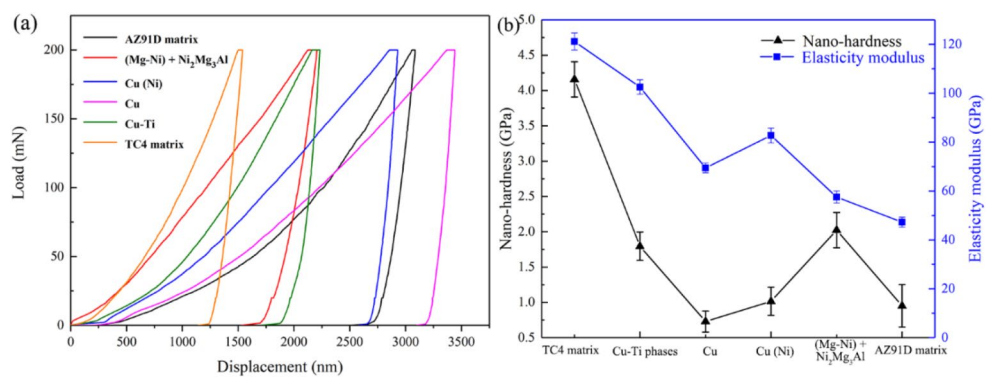

Fig. 10 Nano-indentation test results of the interface microstructure of TC4/(Cu/Ni)/AZ91D bimetals: (**a**) P-h curves, (**b**) nano-hardness and elasticity modulus

3.5 Mechanical Properties of TC4/AZ91D Bimetal

Figure 9 exhibits the optical images and laser confocal images of indentation morphology of the interface microstructure of TC4/(Cu/Ni)/AZ91D bimetals. As shown, the indentation morphology of **P1-P6** were located on AZ91D matrix, ($Ni_2Mg_3Al+(\alpha\text{-}Mg+Mg_2Ni)$) mixed structure, Cu (Ni) solid solution, residual Cu layer, Cu-Ti reaction layers and TC4 matrix, respectively. In order to evaluate ability of these interface structures to resist deformation, the pressure mark morphology of these interface structures were also measured by laser confocal microscope. As shown, the size and depth of the indentation on the residual Cu layer is largest, indicating that the ability of the resistance deformation for this part is weak. However, the size and depth of the pressure marks on the matrix of ($Ni_2Mg_3Al + (\alpha\text{-}Mg+Mg_2Ni)$) and TC4 are relatively minimal, indicating that these two regions have higher nano hardness values.

Figure 10a shows the nano-hardness and elasticity modulus of IMCs generated at the interface region of TC4/(Cu/Ni)/AZ91D bimetals. As shown, the nano-hardness value of TC4 and AZ91D is 4.2 GPa and 0.9 GPa (Table 4), respectively, which is in accordance with several studies [23–26]. However, the nano-hardness and elasticity modulus of ($Mg_2Ni + Ni_2Mg_3Al$) reaction layer is 2.1 GPa and 58 GPa (Table 4), which are lower than that of TC4 matrix but higher than that of AZ91D matrix. However, for the Cu(Ni) solid solution reaction layer, the nano-hardness of it reaches 1.2 GPa (Table 4), which is close to that of AZ91D matrix. However, the elasticity modulus of it reaches 82.7 GPa) (Table 4), which is far higher than that of AZ91D matrix. As for Cu-Ti phases reaction layers, both the nano-hardness (1.8 GPa) and elasticity modulus (103 GPa) are slightly higher than that of AZ91D matrix but far lower than that of TC4 substrate (Table 4). It's worth noting that .the nano-hardness of Cu-Ti phase reached about 3-5.5 GPa in the study of Cai et al. [27], which is slightly higher than the

Table 4 The nano-hardness and elastic modulus of interface microstructure of TC4/AZ91D bimetals

Interface region	H/GPa	E/GPa	Interface region	H/GPa	E/GPa
AZ91D	0.9	12	Cu-Ti IMCs	1.8	103
$Mg_2Ni + Ni_2Mg_3Al$	2.1	58	Ni-Ti IMCs	6.4	149
$Ni_2Mg_3Al + Al_3Ni$	2.5	112	β-Ti	5.7	115
Cu	0.68	70	TC4	4.2	118
Cu(Ni)	1.2	82	Al_3Ni	1.61	73.7

results of this study. The cause of this phenomenon may be the residual Cu layer on the right side of Cu-Ti phase reaction layers.

Figure 11 exhibits the optical images and laser confocal images of indentation morphology of the interface microstructure of TC4/(Ni/Cu)/AZ91D bimetals. As shown, the indentation morphology of P1-P6 were located on granular

Al_3Ni, $(Ni_2Mg_3Al + Al_3Ni)$ mixed structure, Ni-Ti reaction layers and TC4 matrix, respectively. The pressure mark morphology of these interface structures were also measured by the laser confocal microscope. As shown, both the size and depth of the indentations on the interface region were significantly reduced compared to the case of using Cu/Ni composite interlayer. Therefore, it can be inferred that the ability of interface microstructure to occur plastic deformation is also difficult in this case.

Figure 12 illustrates the nano-hardness and elasticity modulus test results of IMCs generated at the interface region of TC4/AZ91D bimetals using Ni/Cu composite interlayer. As shown, the **P1** indentation was assigned on the Al_3Ni reaction layer, the nano-hardness and elasticity modulus of Al_3Ni reaction layer is 1.61 GPa and 73.7 GPa (Table 4), which are much higher than that of AZ91D matrix. Compared to the particles of Al_3Ni, the nano-hardness of mixed tissue of $(Al_3Ni + Ni_2Mg_3Al)$ reached 2.5

Fig. 11 The indentation morphology of the interface microstructure of TC4/(Cu/Ni)/AZ91D bimetals: (**a**) optical images, (**b**)-(**g**) laser confocal morphology
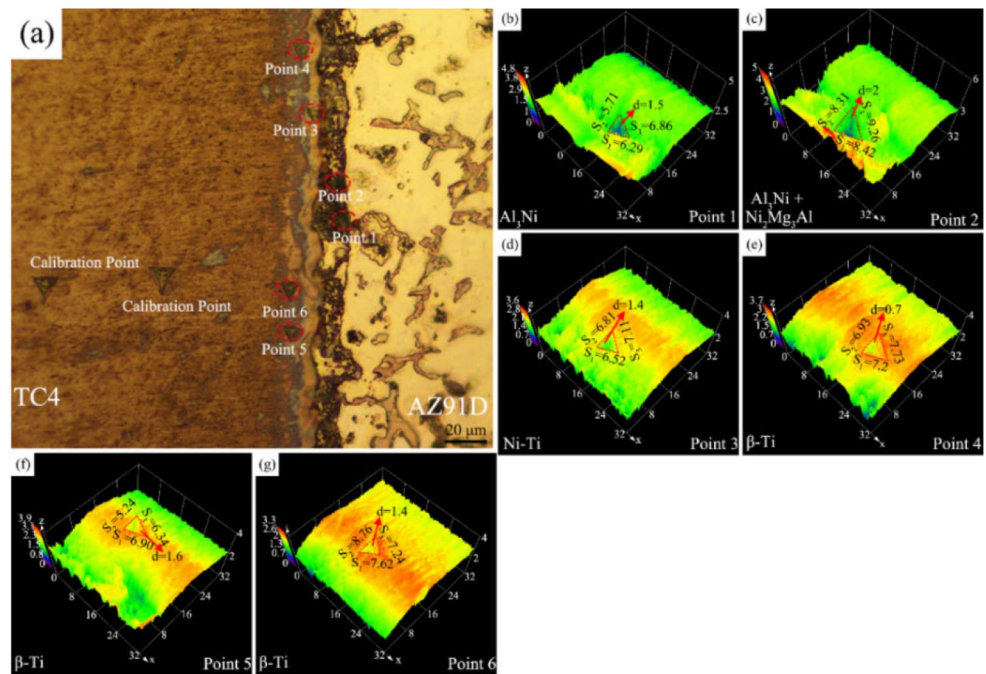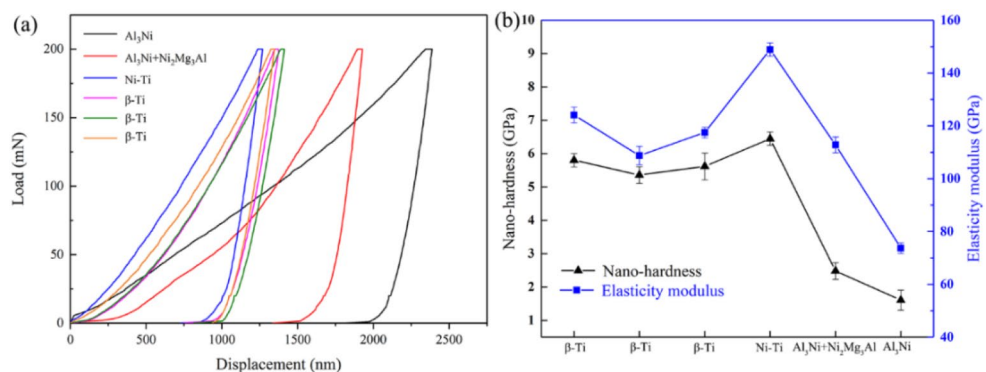

Fig. 12 Nano-indentation test results of the interface microstructure of TC4/(Ni/Cu)/AZ91D bimetals: (**a**) P-h curves, (**b**) nano-hardness and elasticity modulus
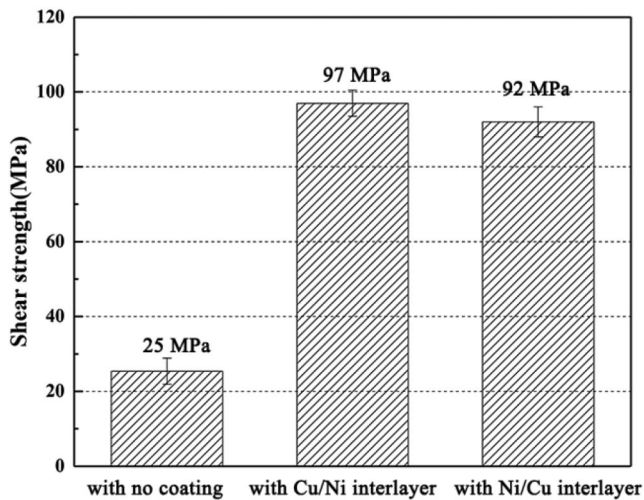
Fig. 13 Shear test results of TC4/AZ91D bimetals using Cu-Ni composite interlayer

GPa (Table 4), which is higher than that of Al_3Ni phase but far less than Ni-Ti IMCs.

The shear strength of the TC4/AZ91D bimetals were also discussed in this study. As can be seen in Fig. 13, the shear strength of TC4/AZ91D bimetal using Cu/Ni composite interlayer reached 97 MPa, which is e only 5 MPa higher than using a Ni/Cu composite interlayer. However, shear strength of TC4/AZ91D bimetals without any interlayers only reached 25 MPa in our previous study [19], thus substantiate the effectiveness of the Cu-Ni composite interlayers. According to the microstructure evolution and nanoindentation test of interface region above, the difference of shear strength at interface region can be ascribed to undesirable effect of interface reaction products on shear strength.

Figure 14 shows the fracture morphology of TC4/AZ91D bimetals that were manufactured using Cu/Ni and Ni/Cu composite interlayer. There were a few flat river patterns in the fracture surface of TC4/AZ91D bimetals using Cu/Ni composite interlayer (Fig. 14b). Furthermore, cross section observation and EDS results illustrating that fracture mainly occurred within $(Ni_2Mg_3Al + (\alpha\text{-}Mg + Mg_2Ni)$ mixed reaction layer (Fig. 14a, c and d). Integrated to nanohardness and elasticity modulus test above, the elasticity modulus of $(Ni_2Mg_3Al + (\alpha\text{-}Mg + Mg_2Ni)$ was the least but the nano-hardness of it was the highest among Cu(Ni) solid solution, residual Cu interlayer and Cu-Ti IMCs layers, indicating that stress concentration was caused easily in this region during shear process. In addition, the $(Ni_2Mg_3Al + (\alpha\text{-}Mg + Mg_2Ni)$ has the maximum width of the reaction layer within the interface of TC4/(Cu/Ni)/AZ91D bimetals. Hence, the probability of breaking failure is also the largest.

In addition, the fracture surface of the TC4/AZ91D cast using Ni/Cu composite interlayer was flat (Fig. 14f). According to EDS results, the polyhedral grain fracture morphology in the interfacial zone was caused by brittle fracture of Ni_3Ti reaction layer (Fig. 14e, g and f). On the other hand, the ration of micro-hardness dissipate (MDP) of Ni-Ti reaction layers was well below than that of $(Al_3Ni + Ni_2Mg_3Al)$ and Al_3Ni IMCs, and on the other hand, the ability of deformation for Ni_3Ti IMC was poor due to its hcp structure. Therefore, when the interface stress concentration level exceed grain bond strength, the shear fracture tend to occur within Ni_3Ti reaction layer. In contrast, there is no brittle fracture for granular Al_3Ni and $(Al_3Ni + Ni_2Mg_3Al)$ reaction layers, which is consistent to the ration of nano-hardness and elasticity modulus research above.
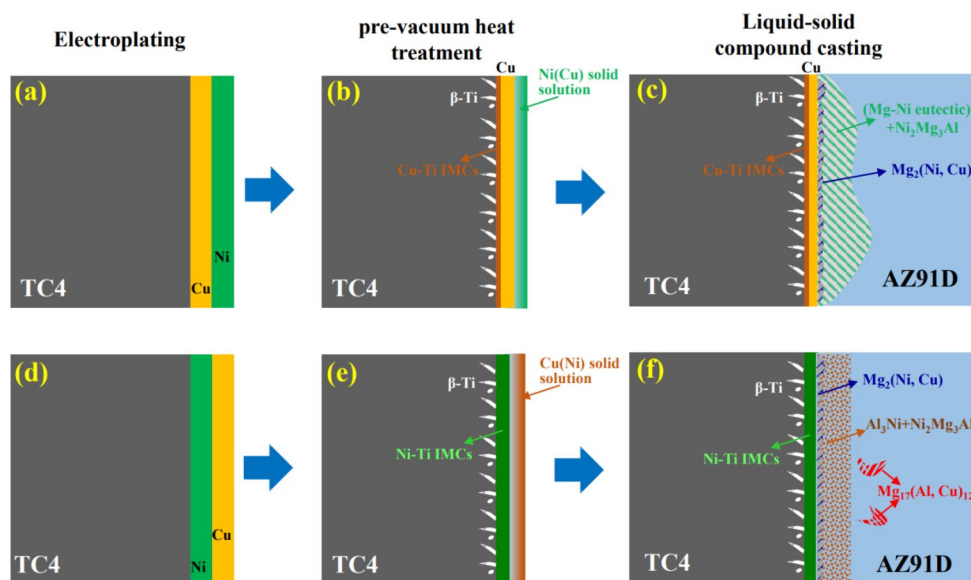

Fig. 14 Fracture analysis of TC4/AZ91D bimetals with Cu-Ni composite interlayer: (a, b) TC4/(Cu/Ni)/AZ91D, (c, d) EDS point scan spectra in a and b, (e, f) TC4/(Ni/Cu)/AZ91D, (g, h) EDS point scan spectra in (e) and (f)
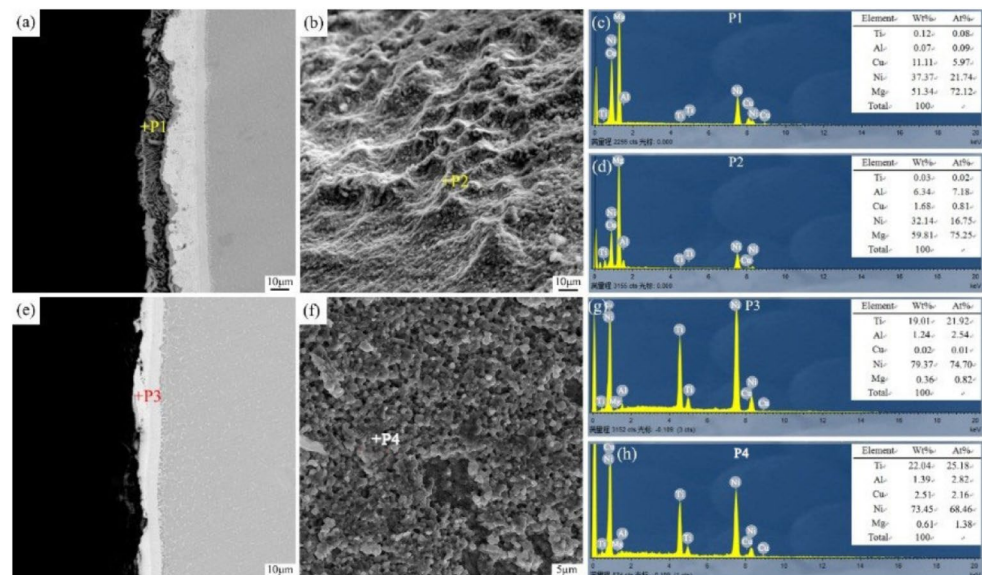
3.6 Interface Formation Mechanism

According to the microstructure evolution, the schematic diagram of interface formation mechanism of TC4/AZ91D bimetals fabricated using Cu/Ni and Ni/Cu composite interlayer is illustrated in Fig. 15. Firstly, the Cu/Ni and Ni/Cu composite interlayers have been performed on the surface of TC4 rod to fabricate TC4/AZ91D bimetals by electroplating. After vacuum heat treatment, both the Cu/Ni and Ni/Cu coated TC4 rods were observed to generate evident diffusion layers at the Cu/Ti and Ni/Ti interface. Meanwhile, significant inter-diffusion is also observed to occur at the interface of Ni and Cu interlayer. According to the Cu-Ni binary phase diagram, there are only Cu(Ni) or Ni(Cu) solid solution can be formed between Cu and Ni elements but have no IMCs [28]. Therefore, the pure Ni and Cu layer on the surface of TC4 rods were replaced by Ni(Cu) and Cu(Ni) solid solution as shown in Fig. 15b. During the liquid-solid compound casting process of TC4/AZ91D bimetal, the AZ91D melt first contacts with Ni(Cu) and Cu(Ni) solid solution. Although the melting temperature of Cu(Ni) and Ni(Cu) solid solution is between 1455 °C and 1083 °C, which is higher than the pouring temperature of AZ91D melt of 720 °C. However, Ni and Cu elements were observed to dissolve into AZ91D melt due to the concentration gradient. For TC4/AZ91D bimetal using Cu/Ni composite interlayer, Ni(Cu) solid solution layer contacts AZ91D melt firstly, although the diffusivity of Ni in Mg ($D_{0\ Ni\ in\ Mg} = 1.2*10^{-9} m^2 s^{-1}$) is lower than that of Cu in Mg ($D_{0\ Cu\ in\ Mg} = 3.039*10^{-3} m^2 s^{-1}$) [29], but the more significant concentration gradient were provided by the Ni(Cu) solid solution for Ni elements to diffuse a long distance. And attributing to the continuous diffusion of the Ni atoms into the AZ91D melt, Mg-Al-Ni ternary phase was formed as illustrated in Fig. 15c.

The Gibbs free energy of Mg-Al-Cu and Mg-Al-Ni ternary system were also calculated to research the order of the metallurgical reaction, and the calculation process and calculation parameters such as temperature and so on are referred to the previous study [21, 22]. As can be seen, due to a lower Gibbs free energy (ΔG) of Mg-Cu phase in Fig. 16a, the Mg_2Cu layer formed at the surface of Ni(Cu) solid solution firstly by the reaction: $L \xrightarrow{487°C} \alpha\text{-Mg} + Mg_2Cu$. And due to the generation of this Mg_2Cu layer, the further diffusion of Cu and Ni elements into AZ91D melt were prevented, thus resulting in the residual of Ni(Cu) solid solution at the interface region. For TC4/AZ91D bimetals using Ni/Cu composite interlayer, Cu(Ni) solid solution layer contacts AZ91D melt firstly, due to a lower melting point and faster diffusion velocity of Cu atoms in Cu(Ni) solid solution, the $Mg_{17}(Al, Cu)_{12}$ phase was observed to generate at a far distance from the interface. In addition, the rapid dissolution of copper atoms in AZ91D melt caused the Cu(Ni) solid solution to transform into a multi-hole structure. Resultantly, the diffusion reaction between Ni elements and AZ91D substrate was gradually enhanced, and granular ($Al_3Ni + Ni_2Mg_3Al$) mixed structure generated at interface area due to a lower Gibbs free energy (ΔG) of Al-Ni phase and Mg-Al-Ni ternary phase in Fig. 16b.

4 Conclusions

In this paper, the Cu-Ni and Ni-Cu composite interlayer were used to achieve AZ91D/TC4 bimetals by LSCC process. The diffusion process of metal atoms and the formation of intermetallic compounds at the interface of Mg/Ti bimetal was also studied. Cu-Ti intermetallic compounds

Fig. 15 Schematic of bonding mechanism of TC4/AZ91D bimetal using Cu-Ni composite interlayer: (**a**)-(**c**) Cu/Ni; (**d**)-(**f**): Ni/Cu

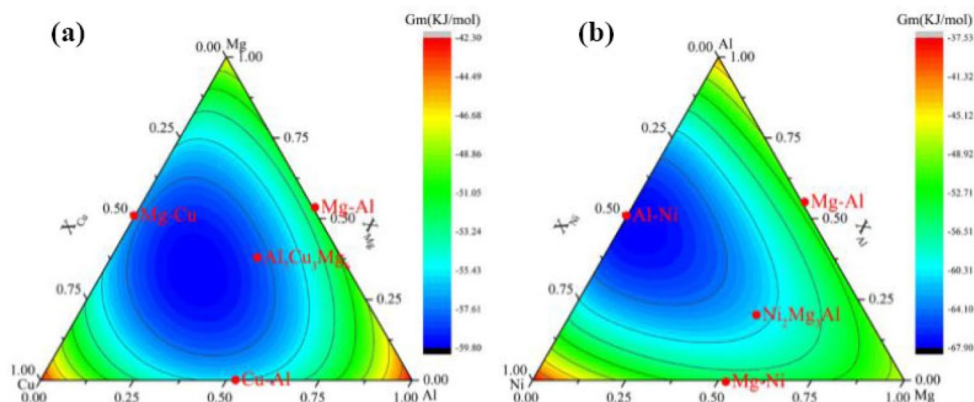**Fig. 16** Gibbs free energy of (**a**) Mg-Al-Cu system, (**b**) Al-Mg-Ni system

exhibit more excellent comprehensive mechanical properties than Ni-Ti intermetallic compounds. The conclusions are as follows:

(1) The Cu-Ni and Ni-Cu composite interlayer was prepared on the surface of TC4 alloy by electroplating. Due to a higher electroplating rate of Cu atoms on TC4 matrix, the thickness of Cu-Ni is thicker than that of Ni-Cu composite interlayer. When treated at 700 °C for 3 h, the interface of TC4/(Cu/Ni) consists of Cu-Ti phases, Cu interlayer and Ni (Cu) solid solution, but the interface of TC4/(Ni/Cu) consists of Ni-Ti phases and Cu (Ni) solid solution.

(2) Metallurgical bonding of TC4/AZ91D can be obtained both using Cu/Ni and Ni/Cu composite interlayer. When using Cu/Ni composite interlayer, the width of about 100 μm of interface obtained, consisting of Cu-Ti, Mg-Al-Ni and Mg-Ni phase. However, when using Ni/Cu composite interlayer, the width of about 40 μm of interface formed, composing of Ni-Ti, Al-Ni, Mg-Al-Ni and Mg-Al-Cu phases.

(3) The interface shear strength and nano-hardness of TC4/AZ91D bimetal were also measured. Since the nano-hardness and elasticity modulus of interface IMCs when using Cu/Ni interlayer gradually decreases from TC4 to AZ91D matrix, but Ni-Ti phases has higher value of nano-hardness than TC4 matrix when using Ni/Cu interlayer, therefore, more excellent comprehensive properties of interface of TC4/AZ91D using Cu/Ni was obtained. The shear test also shows that the shear strength of TC4/AZ91D bimetal using Cu/Ni and Ni/Cu composite interlayers exhibit comparable strength.

Author contributions All authors had contributed to different aspects of this work. Fulin Wen: Investigation, Date curation, Writing-review & editing, DengZhi Zheng: Writing- review & editing. Jianhui Liu: Investigation, Writing-original draft.

Declarations

References

1. Z. Yan, Y. Yu, J. Qian, J. Luo, Y. Sang, Met. Mater. Int. **27**, 4182 (2021). https://doi.org/10.1007/s12540-020-00859-7
2. J. Li, A. Zhang, H. Pan, Y. Ren, Z. Zeng, Q. Huang, C. Yang, L. Ma, G. Qin, J. Magnes Alloy. **9**, 1297 (2021). https://doi.org/10.1016/j.jma.2020.05.011
3. D. Wan, J. Hu, Y. Hu, H. Wang, Met. Mater. Int. **26**, 69 (2020). https://doi.org/10.1007/s12540-019-00302-6
4. J. Lee, D. Seo, H. Chang, Met. Mater. Int. **27**, 3095 (2021). https://doi.org/10.1007/s12540-021-01085-5
5. C. Qi, Y. Du, P. Yang, Z. Liu, H. Lyu, K. Zhao, L. Guo, Met. Mater. Int. **28**, 3068 (2022). https://doi.org/10.1007/s12540-022-01181-0
6. Z. Zhang, C. Tan, G. Wang, B. Chen, X. Song, H. Zhao, L. Li, J. Feng, J. Mater. Eng. Perform. **27**, 1414 (2018). https://doi.org/10.1007/s11665-018-3196-y
7. M. Aonuma, T. Tsumura, K. Nakata, J. Jpn Inst. Light Met. **57**, 112 (2007). https://doi.org/10.2464/jilm.57.112
8. M. Gao, Z. Wang, X. Li, X. Zeng, Metall. Mater. Trans. A **43**, 163 (2012). https://doi.org/10.1007/s11661-011-0825-6
9. R. Cao, T. Wang, C. Wang, Z. Feng, Q. Lin, J. Chen, J. Alloys Compd. **605**, 12 (2014). https://doi.org/10.1016/j.jallcom.2014.03.051
10. V. Lopes, H. Puga, I. Gomes, N. Peixinho, J. Teixeira, J. Barbosa, J. Mater. Process. Technol. **299**, 117339 (2022). https://doi.org/10.1016/j.jmatprotec.2021.117339
11. S. Li, D. Li, X. Zeng, W. Ding, Trans. Nonferr. Met. Soc. China **24**, 3769 (2014). https://doi.org/10.1016/S1003-6326(14)63531-7
12. F. Wang, N. Wang, F. Yu, X. Wang, J. Cui, J. Alloys Compd. **820**, 153318 (2020). https://doi.org/10.1016/j.jallcom.2019.153318
13. K. Zhang, J. Liu, C. Tan, G. Wang, X. Song, B. Chen, L. Li, J. Feng, J. Manuf. Process. **34**, 148 (2018). https://doi.org/10.1016/j.jmapro.2018.05.037
14. A.M. Atieh, T.I. Khan, Sci. Technol. Weld. Join. **19**, 333 (2014). https://doi.org/10.1179/1362171814Y.0000000196
15. C. Zang, J. Liu, C. Tan, K. Zhang, X. Song, B. Chen, L. Li, J. Feng, J. Manuf. Process. **32**, 595 (2018). https://doi.org/10.1016/j.jmapro.2018.03.019
16. J. Liu, C. Tan, L. Wu, X. Zhao, Z. Zhang, B. Chen, X. Song, J. Feng, Opt. Laser Technol. **117**, 200 (2019). https://doi.org/10.1016/j.jmapro.2018.03.019

17. S. Auwal, S. Ramesh, Z. Zhang, F. Yusof, J. Liu, C. Tan, S. Man-ladan, F. Tarlochan, Opt. Laser Technol. **115**, 149 (2019). https://doi.org/10.1016/j.jmapro.2018.03.019

18. C. Wang, H. Wang, F. Geng, C. Gang, L. Cui, P. Zhang, Mater. Sci. Eng. A **714**, 14 (2018). https://doi.org/10.1016/j.msea.2017.12.017

19. F. Wen, J. Zhao, M. Yuan, J. Wang, D. Zheng, J. Zhang, K. He, J. Shangguan, Y. Guo, J. Magnes Alloy. **9**, 1382 (2021). https://doi.org/10.1016/j.jma.2020.05.021

20. F. Wen, J. Zhao, K. Feng, M. Yuan, D. Zheng, C. Gu, B. Xu, Met. Mater. Int. **28**, 1711 (2022). https://doi.org/10.1007/s12540-021-01027-1

21. X. Lv, L. Liu, G. Song, J. Manuf. Process. **83**, 678 (2022). https://doi.org/10.1016/j.jmapro.2022.09.034

22. G. Song, G. An, L. Liu, Mater. Des. **35**, 323 (2012). https://doi.org/10.1016/j.matdes.2011.09.006

23. W.H. Kao, Y.L. Su, J.H. Horng, C.Y. Chang, Surf. Coat. Tech. **350**, 172 (2018). https://doi.org/10.1016/j.surfcoat.2018.07.011

24. F. Bartolomeu, M. Costa, N. Alves, G. Miranda, F. Silva, Opt. Laser Eng. **134**, 106208 (2020). https://doi.org/10.1016/j.optlaseng.2020.106208

25. T. Yao, K. Wang, H. Yang, H. Jiang, J. Wei, W. Wu, H. Liu, Q. Wang, W. Ding, Materials. **14**, 1407 (2021). https://doi.org/10.3390/ma14061407

26. G. Li, W. Jiang, F. Guan, J. Zhu, Z. Zhang, Z. Fan, J. Mater. Process. Tech. **288**, 116874 (2021). https://doi.org/10.1016/j.jmatprotec.2020.116874

27. Q. Cai, W. Liu, Y. Ma, W. Zhu, X. Pang, J. Nucl. Mater. **507**, 198 (2018). https://doi.org/10.1016/j.jnucmat.2018.05.004

28. I. Mizushima, M. Chikazawa, T. Watanabe, J. Electrochem. Soc. **143**, 1978 (1996). https://doi.org/10.1149/1.1836935

29. A.M. Atieh, T.I. Khan, J. Mater. Sci. **49**, 7648 (2014). https://doi.org/10.1007/s10853-014-8473-z